The Andromeda Galaxy's most important merger was with M32's progenitor ~2 Gyr ago

Richard D'Souza* & Eric F. Bell

The Andromeda Galaxy (M31), our nearest large galactic neighbour, offers a unique opportunity to test how mergers affect galaxy properties[1]. Although attempts have been made to simulate the interaction of existing satellites or their remnants with M31 using limited phase-space information[2,3,4], the most informative tracers of M31's merger history are its outer low surface brightness regions (its stellar halo), which is caused mainly by the tidal disruption of satellite galaxies[5]. Here we use cosmological models of galaxy formation[6,7] to show that M31's massive[8] and metal-rich[9] stellar halo containing intermediate age stars[10,11] implies that it merged with a large ($M_* \sim 2.5 \times 10^{10} M_\odot$) galaxy ~2 Gyr ago. The simulated properties of the merger debris help to interpret a broader set of observations of M31's stellar halo and satellites than previously considered: its compact and metal-rich satellite M32 is the tidally-stripped core of the disrupted galaxy, M31's rotating and flattened inner stellar halo[12] contains most of the merger debris, and the giant stellar stream[13] is likely to have been thrown out during the merger. This accreted galaxy was the third largest member of the Local Group. This merger may explain the global burst of star formation ~2 Gyr ago[14] in the disk of M31 in which ~1/5 of its stars were formed. Moreover, M31's disk and bulge were already in place before its most important merger, suggesting that mergers of this magnitude do not dramatically affect galaxy structure.

Existing methods for inferring merger history generally simulate the interactions of existing satellites[2,3] (or their remnants[4]) with their host galaxies. Generally, these methods attempt to reproduce limited and often uncertain kinematic information and one or more observational features such as M32's outer isophotes[15], M31's giant stellar stream[4] or M31's star-forming ring[2,3]. The physical drivers of these observational features are often ambiguous or complex, and may not always require a merger origin. In particular, the longevity and lack of expansion with time of the star-forming ring over the last 500 Myr argues against[16] a purely collisional origin[2,3]. Therefore it is unsurprising that these analyses result in contradictory pictures for the merger history of M31 and the interaction between M31 and M32[2,3,4,15]. Yet, because M32 is compact

and metal-rich for its stellar mass, it is generally accepted that it is the core of a previously much more massive satellite[17]. Furthermore, potentially important constraints are often not included, such as the extended star formation history of M32[18] which strongly suggests an origin by stripping of a gas-rich satellite[19]. Since M31's stellar halo should be the reservoir of much of M32's stripped material, measurements of its halo[8–12] can give previously unavailable and decisive guidance to distinguish between M32's formation scenarios and possible progenitors as well as to reconstruct M31's merger history.

Our inability to extract an accretion history from M31's stellar halo boils down to a disagreement about how many satellites dominate its halo. Existing theoretical models based on the low-mass Milky Way stellar halo[5] suggested that halos should be built up from several 10^7-10^9 $M_\odot$ progenitors, including the progenitors of the Giant Stellar Stream and M32. However, similarities in the stellar populations[10,11] between different parts of the metal-rich, rotating[12] inner stellar halo suggested that the *entire* inner stellar halo might be accreted from a single satellite galaxy[12]. Furthermore, stars stripped from the M31's disk found in the inner stellar halo[11] further complicates the identification of the progenitors. The lack of agreement about how many progenitors dominate M31's halo has prevented a coherent interpretation of the most significant features of M31's stellar halo and the responsible merger event(s).

Cosmological models of galaxy formation encoding a diversity in accretion histories show that galaxies with a massive stellar halo (as large as M31's) are dominated by a single massive merger and that its outer stellar halo is dominated by accreted stars[20]. This allows us to frame three central questions. a) How does M31's massive[8] and metal-rich[9] outer stellar halo (>27 kpc) constrain the mass, type and time of accretion of the most-massive merger? b) Which observational features of M31 are consistent with the debris of such an event? c) Can these features allow us to further constrain the timing of the merger and the type of progenitor?

Simulated galaxies from two independent set of cosmological simulations[6,7] with M31's stellar mass and virial mass are predicted to have a wide range of accreted masses and consequently a wide range of masses, metallicities and accretion times of the most massive progenitors (Fig. 2). Adding the extra constraint of a large accreted stellar component ($M_{*acc} > 2 \times 10^{10}$ $M_\odot$) isolates

true 'M31 analogues' with a much narrower range of accretion histories: M31 analogues invariably have *massive* ($10^{10} < M_* / M_\odot < 10^{11}$) and *metal-rich* (-0.2<[M/H]<0.2) progenitors accreted in the *last ~5 Gyr.* The high metallicity of M31's accreted stellar component argues that a single progenitor completely dominates M31's accreted mass budget. These massive progenitors are in general star-forming, gas-rich, rotating galaxies with well-established metallicity gradients.

We use M31 analogues from a hydrodynamical simulation to illustrate the merger process and its likely debris field. As the merger progresses towards the right in Fig. 3, the satellite galaxy is disrupted, leading to a burst in star formation. The cessation in centrally-concentrated star formation occurs shortly before coalescence with the main galaxy. Most of the satellite is disrupted into a structured but highly-flattened rotating inner stellar halo with an exponential density profile along the major axis, a $R^{1/4}$ profile along the minor axis, and a velocity dispersion that drops towards larger radius. The debris field is metal-rich. Gradients in the progenitor result in the stellar halo having variations in metallicity by a factor of 10 and time of star formation shut-off by > 2 Gyr, with the most metal-rich and youngest parts concentrated towards the center. In most cases, a prominent metal-rich tidal stream is frequently produced.

The observational features most consistent with the metal-rich debris of M31's massive progenitor are M32, the inner stellar halo and the giant stellar stream, while excluding the other metal-poor satellites and streams that are expected to be from numerous smaller accretion events[5]. We now use these features to further constrain the type of progenitor and the timing of the merger.

M32: M32's compact size, solar metallicity and sizeable intermediate-age stellar populations are easily explained if it is the compact core of M31's massive (~2.5×10^{10} $M_\odot$) gas and metal rich accreted progenitor (Fig. 2) which we term as **M32p**. M32p is likely to have experienced late star formation triggered by gas inflow to the center of the galaxy as it is being accreted (Fig. 3a, top right)[21], similar to the observed star formation experienced by M32 ~2-5 Gyr ago (Fig. 1, top left)[18]. The timing of the starburst suggests that M32p started interacting with M31 approximately 5 Gyr ago, and that its disruption continued until around 2 Gyr ago. The presence

of a massive central black hole ($3.4 \pm 1.6 \times 10^6$ $M_\odot$[22]) suggests a relatively low upper limit on the mass of the bulge of M32p ($M_{Bulge} < 5.9 \times 10^9$ $M_\odot$ using the scatter in the black-hole mass-bulge mass relationship[23]), consistent with qualitative arguments of why M32 did not sink to center of M31 due to dynamical friction.

Inner stellar halo: M32p's tidally-stripped debris can explain most of the properties of M31's metal-rich inner stellar halo (see Figs. 1-3), including its flattened spheroidal nature, its disk-like rotation[12], the presence of intermediate-age stars and some of its stellar population variations[10,11] (Fig. 3). M32p's debris dominates the minor axis density profile of M31 from a projected distance of ~8 kpc out to 25 kpc[24,25] (see inset of Fig 3a). We conclude that M31's inner stellar halo contains the majority of M32p's debris, with a possible contribution from in-situ stars kicked up by the merger[11]. The cessation of star formation ~2 Gyr ago in M31's inner stellar halo[10,11] (Fig. 1) agrees with the inferred merger time between M32p and M31.

Giant stellar stream: Large metal-rich tidal streams are frequently produced by the most-massive satellite. Since M31's giant stellar stream has a metallicity and recent star formation history similar to M31's inner stellar halo (Fig. 1), we suggest that it is likely that the giant stellar stream is from M32p's tidal disruption. If so, the kinematics of the giant stellar stream allows one to put further constraints on its possible progenitor. Dynamical models[4] show that debris from the progenitor of the giant stellar stream lies in M31's inner stellar halo, concentrated between the North east and the Western shelves of M31. While the remnant is predicted to lie within a constrained region of position-radial velocity space, quantitative predictions are affected by systematic uncertainties in the model. M32, the core of M32p, lies within this region of position-velocity space predicted by the model. If the GSS is associated with M32p as its progenitor, then the orbits of the dynamical models[4] would suggest a last pericenter time of ~1.5 Gyrs and a pericenter mass > 5×10^9 $M_\odot$. These revised dynamical constraints agree with the independent mass estimates for M32p from M32's stellar metallicity as well as from the accreted stellar mass constraints of M31. Moreover, the revised time of pericentric passage is in accord with measurements of a synchronous star formation burst around 2 Gyr ago evident in the stellar populations of the GSS, M32 and the inner stellar halo, suggesting that the GSS is indeed likely to have been produced by M32p's merger with M31.

In addition to laying out a framework for characterizing the most massive merger events in other galaxies, there are three interesting implications of this work for our understanding of M31. Firstly, because M31's disk pre-dates this interaction[14], M31's disk survived a merger with mass ratio between ~0.1 and ~0.3. Second, while M31's disk survived, it may have been thickened to its present scale height of ~1 kpc[26] by this merger and experienced a galaxy-wide star formation episode around 2 Gyr ago in which ~1/5 of its stars formed[14]. If indeed this episode is associated with its merger with M32p, this provides the first empirical measurement of the lifecycle effects of such a merger. Finally, large bulges like M31's have been suggested to have been made in galaxy mergers[1]. Yet, M31 had already formed its bulge stars >6 Gyr ago[27], long before M31's merger with M32p. This adds to the evidence[28] that merging and bulge formation are not trivially linked.

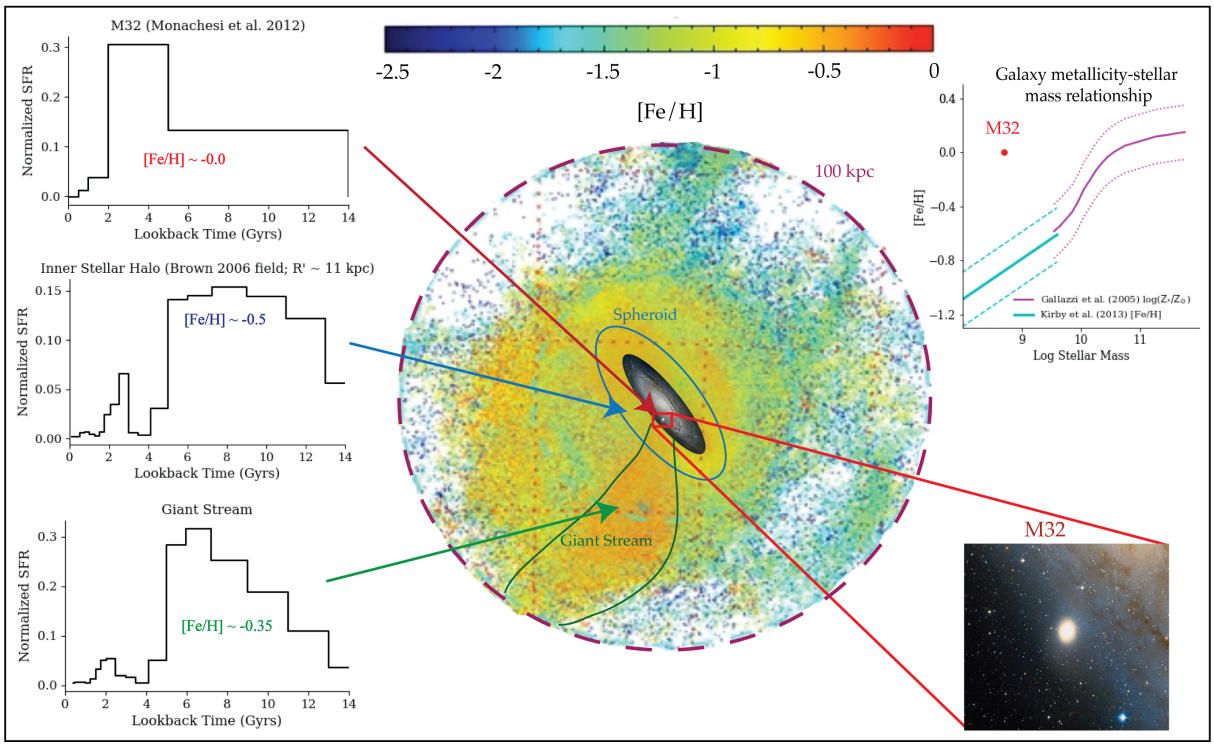

Figure 1: **The stellar halo of M31** is massive, extensive, extremely-metal rich and has a substantial population of young and intermediate-aged stars. The giant stellar stream shows a similar range in stellar populations. M32, a compact and metal-rich satellite of M31 is deeply embedded in M31's inner stellar halo. The intensity scale of the metallicity map[4] codes the density of stars and the color denotes the typical metallicity of the halo stars. In particular, three features are highlighted with their respective star formation histories: (top) M32[18] with a half-light radius of 100 pc, (middle) M31's inner stellar halo[11] - its stellar halo out to ~30 kpc along the minor axis - and (bottom) the giant stellar stream[11]. The inset on the right demonstrates that the metallicity of M32 is much higher than galaxies with similar mass using the galaxy metallicity-stellar mass relationship[29,30]. The dashed lines in the inset show a 0.18 dex scatter in the relationship. The metallicity map of the stellar halo of M31 is reproduced with permission of the authors[4]. Credits of images of M32 and M31: Wikisky.

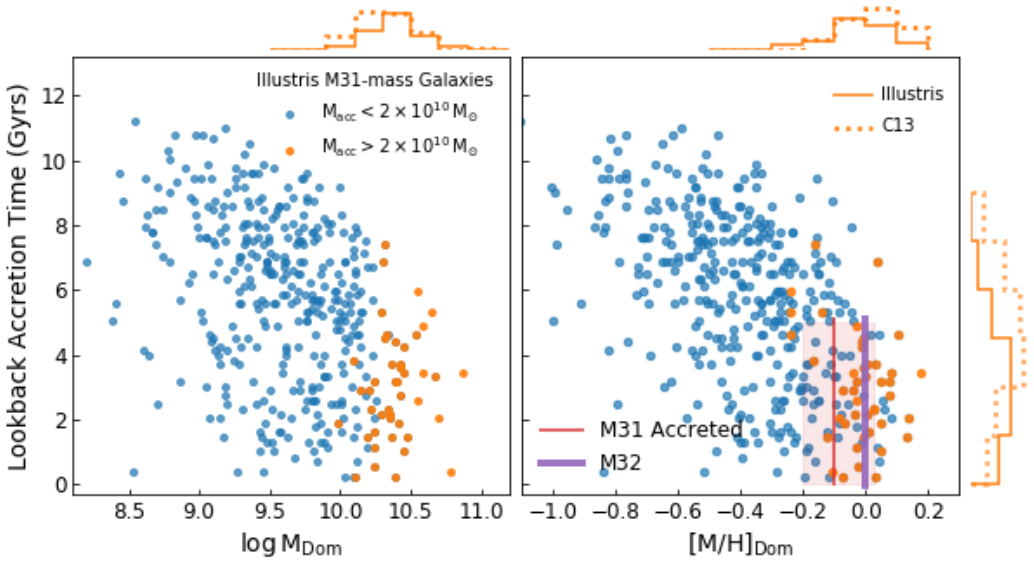

Figure 2: **Constraining the properties of the most massive satellite accreted by M31 analogues**: The large accreted stellar component of M31 ($M_{*,acc}$> 2 x 10^{10} $M_\odot$; see Supplement Sec. 3 for derivation of lower-mass limit of M_{*acc} from observations of the outer stellar halo[8] of M31 beyond a projected radius of 27 kpc) strongly constrains the possible massive progenitors of M31 analogues (orange symbols) to be massive $10^{10} < M_{Dom}/M_\odot < 5 \times 10^{10}$, metal rich -0.2<[M/H]<0.2, and accreted late in the last ~5 Gyr. The most massive accreted progenitors of M31 analogues are studied using two independent cosmological galaxy formation models - the Illustris hydrodynamical simulation[6] (solid orange histogram) and a semi-analytic particle-tagging analysis[7] of the Millennium-II simulation (dotted orange histograms, called C13 in the Figure). The union of the blue and orange symbols show the properties of the most massive progenitors of the complete set of M31-mass galaxies from the Illustris simulations with 1.1 x $10^{12} < M_{virial}/M_\odot < 2.24 \times 10^{12}$, 5 x $10^{10} < M_*/M_\odot < 2 \times 10^{11}$ and accreted stellar fraction f_{acc}< 0.5, showing the full range of possible accretion histories, of which the orange symbols show the subset with large accreted stellar components. We plot the lookback accretion time of the most massive accreted progenitors as a function of its stellar mass (log M_{Dom}) and metallicity ($[M/H]_{Dom}$). The subset of M31-mass galaxies with massive observed stellar halos result from a constrained subset of massive metal-rich progenitors. M32's stellar metallicity is indicated, with a constraint on the time of accretion derived from the presence of intermediate age stars[18]. Constraints on the metallicity of the accreted stellar component of M31 are derived from the stellar halo metallicity gradient along M31's minor axis[9].

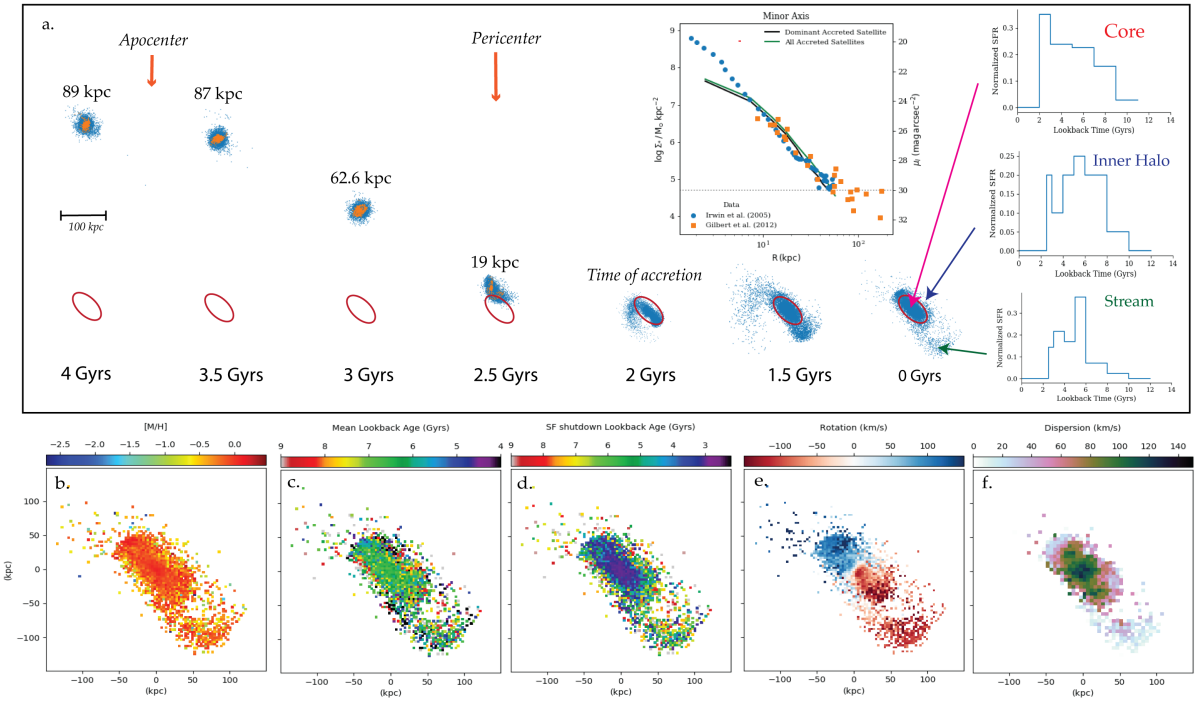

Figure 3: **The progression of the tidal disruption of the most massive progenitor; the properties of its debris appears similar to the stellar halo of M31** (see Fig. 1). a) The progression of the tidal disruption of a massive satellite and its contribution to the stellar halo of an M31-analogue from the Illustris simulation. Blue signifies all the stellar particles of the satellite. The orange signifies those stellar particles that experienced star formation in the last 0.5 Gyr of the time indicated below, showing its centrally-concentrated star formation. The red ellipse signifies the position of the inner stellar halo at z=0, and has a semi-major axis length of 40 kpc. We show the star formation histories of the core, the inner stellar halo and the stream comparable to the observations shown in Fig. 1. The inset shows the median stellar mass surface density profile along the minor axis contributed by the most massive accreted progenitor (solid black line) as well as contributed by all the accreted satellites (solid green line) of the M31 analogues from the Illustris simulations. We also compare this with the data of M31, the i-band surface brightness measurements[24,25] along the minor axis assuming a fiducial M/L ratio in the *i*-band ratio of 1.8. ($M_{\odot}^{i} = 4.53$). The horizontal dotted line is the mass resolution limit of the simulations. The remaining panels show the distribution of the properties of the debris from the massive satellite: b) metallicity map showing a wide range of metallicities, rich structure and a metal-rich stream (compare with the metallicity map in Fig. 1), c) the mean age of stars showing significant variations across the face of the debris field, d) the time of shut down of star formation, showing that the whole debris field formed stars late but the inner parts formed stars for the longest, e) the average velocity of the stars showing strong rotation signatures, and f) the velocity dispersion around that average, showing a strong decline towards its outer parts and a stream with a low velocity dispersion. In all panels, the viewing geometry is similar to our view of M31 to simplify qualitative comparison with observations. Note that the resolution and the softening of the Illustris simulations does not allow us to resolve compact M32-like bound cores of the disrupted satellite.

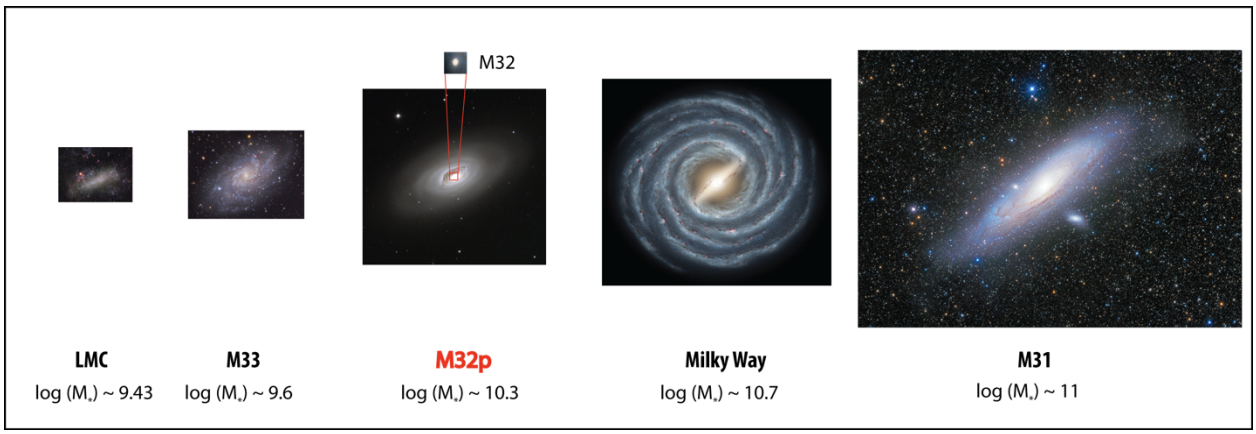

Figure 4: M32p, the most massive progenitor accreted by M31 in relation with the largest of the current Local Group members (LMC, M33, MW and M31). We have represented M32p using an analogue in the local universe M64. The MW is shown through an artist's representation. Credits: LMC, M33 & M31 (Wei-Hao Wang; with permission), MW(NASA/JPL), M64 (NOAO/AURA/NSF)

References:

1. Sommerville & Dave. Physical Models of Galaxy Formation in a Cosmological Framework, ARAA, **53**, 51-113 (2015).
2. Block et al. An almost head-on collision as the origin of two off-centre rings in the Andromeda galaxy, *Nature*, **443**, 832-834 (2006).
3. Dierickx, Blecha & Loeb, Signatures of the M31-M32 Galactic Collision, *Astrophys. J.*, **788**, 38-44 (2014).
4. Fardal et al. Inferring the Andromeda Galaxy's mass from its giant southern stream with Bayesian simulation sampling, *Mon. Not. R. Astron. Soc.*, **434**, 2779-2802 (2013).
5. Bullock & Johnston. Tracing Galaxy Formation with Stellar Halos. I. Methods, *Astrophys. J.*, **635**, 931-949 (2005).
6. Vogelsberger et al. Properties of galaxies reproduced by a hydrodynamic simulation, *Nature*, **509**, 177-182 (2014).
7. Cooper et al. Galactic accretion and the outer structure of galaxies in the CDM model, *Mon. Not. R. Astron. Soc.*, **434**, 3348-3367 (2013).
8. Ibata et al. The Large-scale Structure of the Halo of the Andromeda Galaxy. I. Global Stellar Density, Morphology and Metallicity Properties, *Astrophys. J.*, **780**, 128-148 (2014).

9. Gilbert et al. Global Properties of M31's Stellar Halo from the SPLASH Survey. II. Metallicity Profile, *Astrophys. J.*, **796**, 76-96 (2014).
10. Brown et al. The Detailed Star Formation History in the Spheroid, Outer Disk, and Tidal Stream of the Andromeda Galaxy, Astrophysical Journal, *Astrophys. J.*, **652**, 323-353 (2006).
11. Bernard et al. The nature and origin of substructure in the outskirts of M31 - II. Detailed star formation histories, *Mon. Not. R. Astron. Soc*., **446**, 2789-2801 (2015).
12. Ibata et al. On the Accretion Origin of a Vast Extended Stellar Disk around the Andromeda Galaxy, *Astrophys. J*.**, 634**, 287-313 (2005).
13. Ibata et al. A giant stream of metal-rich stars in the halo of the galaxy M31, *Nature*, **412**, 49-52 (2001).
14. Williams et al. A Global Star-forming Episode in M31 2-4 Gyr Ago, *Astrophys. J.*, **806**, 48-57 (2015).
15. Choi et al. Tidal interaction of M32 and NGC205 with M31: Surface Photometry and Numerical Simulations, *Astron. J.*, **124**, 310-331 (2002).
16. Lewis et al. The Panchromatic Hubble Andromeda Treasury. XI. The Spatially Resolved Recent Star Formation History of M31, *Astrophys. J.*, **805**, 183-204 (2015).
17. Faber, S. Tidal Origin of Elliptical Galaxies of High Surface Brightness, *Astrophys. J.*, **179**, 423-426 (1973).
18. Monachesi et al. The Star Formation History of M32, *Astrophys. J.*, **745**, 97-117 (2012).
19. Bekki et al. A New Formation Model for M32: A Threshed Early-Type Spiral Galaxy? *Astrophys. J.*, **557**, 39-42 (2001).
20. D'Souza & Bell, The masses and metallicities of stellar haloes reflect galactic merger histories, *Mon. Not. R. Astron. Soc*., in press arXiv:1705.08442 (2017).
21. Kewley et al. Metallicity and Nuclear Star Formation in Nearby Galaxy Pairs: Evidence for Tidally Induced Gas Flows, *Astrophys. J.*, **131**, 2004-2017 (2006)
22. van der Marel et al. Improved Evidence for a Black Hole in M32 from HST/FOS Spectra. I. Observations, *Astrophys. J.*, **488**, 119-135 (1997).
23. Haring & Rix, On the Black Hole Mass-Bulge Mass, *Astrophys. J.,* **604**, 89-92 (2004).
24. Irwin et al. A minor axis Surface Brightness Profile of M31, *Astron. J*, **628**, 105-108 (2005).

25. Gilbert et al. Global Properties of M31's Stellar Halo from the SPLASH Survey I. Surface brightness, *Astrophys. J.*, **760**, 76-97 (2012).
26. Dalcanton et al. The Panchromatic Hubble Andromeda Treasury VIII. A wide-field, high-resolution map of Dust extinction in M31, *Astrophys. J.*, **814**, 3-50 (2015).
27. Olsen et al. The Star Formation Histories of the Bulge and Disk of M31 from Resolved Stars in the Near-Infrared, *Astron. J.*, **132**, 271-289 (2006).
28. Bell et al. Galaxies Grow Their Bulges and Black Holes in Diverse Ways, *Astrophys. J.L.*, **837**, 8-13 (2017).
29. Kirby et al. The Universal Stellar Mass-Stellar Metallicity Relation for Dwarf Galaxies, *Astrophys. J.*, **779**, 102-123 (2013).
30. Gallazzi et al. The ages and metallicities of galaxies in the local universe, *Mon. Not. R. Astron. Soc.*, **362**, 41-58 (2005).

Author Contributions: Both authors contributed equally to the work.

Acknowledgments: We would like to thank Julianne Dalcanton, Andrew Cooper, Antonela Monachesi, Scott Trager, Monica Valuri, Kohei Hatori, Kathryn Johnston, Puragra Guhathakurta, Paul Mueller, Joe Wagner and Robert Macke for comments on initial versions of the draft. We thank Andrew Cooper for access to his particle-tagging simulations. We thank Rodrigo Ibata and Karoline Gilbert for permission to use their figures in this publication.

Competing Financial Interests: None

Correspondence: Richard D'Souza (radsouza@umich.edu)

1. Observational Constraints for selecting M31-like galaxies.

The strongest constraints on the *virial mass* of M31 come from the timing argument incorporating the systematic effect of the LMC: $1.33^{+0.39(0.88)}_{-0.33(0.60)}$ x 10^{12} $M_{\odot}$ at a 68% (95%) confidence levels[31]. Constraints from SDSS *ugriz* and Spitzer 3.6 μm imaging suggest that M31's *stellar mass* is 10-15 x 10^{10} $M_{\odot}$[32]. The *mass of the outer stellar halo* (from 27.2 to 150 kpc) assuming an age of 13(9) Gyr is 10.5 (8.8) x 10^{9} $M_{\odot}$.[8]

The metallicity of the total accreted stellar component can be derived from the gradient of the metallicity of M31's stellar halo along the minor axis[20]. This gradient in Fig S1 (in black) was derived using an age of 10 Gyr and an [α/Fe]=0.0[9]. However, there is evidence that the outer stellar halo (>60 kpc) is older in age~10 Gyr, while the inner stellar halo is built up from stars which are considerably younger[10], likely from large satellites accreted fairly recently ([α/Fe]~0.0, Age~5 Gyr). This would make the metallicity gradient steeper than previously estimated (indicative red line in Fig. S1). Extrapolating between the metallicities of the various stellar populations of M31 suggests[20] a median metallicity of $[Fe/H]_{Acc}$ ~ -0.1 +- 0.2 dex for the total accreted stellar component.

2. Models

We use central galaxies from two independent cosmological large-scale galaxy formation models, the Illustris hydrodynamical simulations[6,33,34] and the particle-tagging simulations[7] (hereafter C13) based on the Munich semi-analytic model[35] (hereafter Munich model).

For both simulations, we use only the accreted stellar component which we identify as those particles as those which are formed in subhalos which are not part of the main progenitor branch of the galaxy. The satellite which contributed the most stellar material to the accreted stellar mass of the galaxy is identified as the 'dominant' progenitor. The mass of the satellite is its maximum mass before it is accreted by the main galaxy. We use the median value of the stellar metallicity (all elements above He). The time of accretion of a satellite is when it merges with the main progenitor branch of the galaxy. This corresponds to a time when the satellite cannot be distinguished by the SUBFIND algorithm. Accreted satellites at this stage are usually stripped of most of their stellar material, and are within 100 kpc of the host galaxy. We assume a Hubble parameter of 0.72.

The C13 simulations were run by tagging various fractions of the most-bound DM particles (1, 5 and 10%). C13 found that a tagging fraction of 3-5% best reproduced the observational galaxy stellar mass-radius relationship for late and early type galaxies at z=0[36,37].

3. Radial properties of accretion models

Uncertainties in the predictions of the radial profile of the accreted stellar component affect the extrapolation of the mass of the stellar halo to the total accreted stellar mass. This uncertainty arises primarily due to difference in methodology adopted in the two simulations and the sizes and shapes of the accreted satellites.

We compare the spherically averaged radial profiles of the accreted stellar component of M31-mass galaxies in the two models. We estimate their total accreted stellar mass and the accreted stellar mass beyond a projected galactocentric radius of 27 kpc (Fig S2). For Illustris, we find that the total accreted stellar mass is ~0.5 dex larger than that the accreted stellar mass measured beyond 27 kpc. For C13, assuming a fiducial tagging fraction of 5%, we find that the total accreted stellar mass is ~0.65 dex larger than the accreted stellar mass external to 27 kpc. With a smaller tagging fraction, the accreted stellar material is more centrally concentrated. Furthermore, there appears to be more scatter in the ratio of total accreted stellar mass to the stellar mass beyond 27 kpc in the C13 simulations than in Illustris.

Using both models, we find that the total accreted stellar mass should be at least 0.4 dex larger the mass of the stellar halo outside 27 kpc. Assuming that the mass of the M31's stellar halo beyond 27 kpc is $8.8 \times 10^9\ M_\odot$, we conclude that the total accreted stellar mass of M31 is larger than $2.0 \times 10^{10}\ M_\odot$.

4. Incorporating M33

We choose M31 analogues such that $10.7 < \log M_* < 11.3$, $12.05 < \log M_{DM} < 12.35$, $\log (M_{acc,*}) > 10.3$ and $(M_{acc}/M^*) < 0.5$. We find a total of 44 and 62 galaxies in Illustris & C13 simulations respectively. Imposing that these M31 analogues have also a current satellite of the size of M33 ($\log M^* \sim 9.6$) decreases that number to 11 and 17 galaxies respectively. We conclude that it is not unlikely for M31 to have both a large satellite like M33 as well as having accreted a large progenitor ($\log M^* \sim 10.3$) in the last 5 Gyr.

5. Uniqueness of the massive progenitor

Although the dominant progenitor contributes the majority of the mass to the accreted stellar component of the galaxy, in a few cases for M31-mass galaxies, the second most massive progenitor can be comparable in mass to the dominant progenitor. Yet, M31 analogues with a large accreted stellar component are dominated by a single large progenitor. We calculate the fraction of accreted stellar material contributed by the dominant progenitor ($frac_{Dom}$) as a function of accreted stellar mass for M31-mass galaxies in the Illustris and C13 models (Fig S3). For M31 analogues, $frac_{Dom}$ spans between 0.4 and 1.0 with the mean of the distribution being around 0.8, implying that their stellar halos are built up through the accretion of single large progenitors.

The metallicity of the accreted stellar component can help distinguish between different values of $frac_{dom}$ (Fig S4). If the accreted stellar component is built up from a single dominant event, the metallicity of the accreted stellar component will be relatively high, compared to a galaxy whose accreted stellar component is built up from several smaller accretion events. From the high metallicity of M31's total accreted stellar component ($[M/H]_{acc}>-0.1$) we conclude that it suffered a single large accretion event (larger than $10^{10}\ M_\odot$) in the last 5 Gyr that dominates M31's accreted stellar component. The ratio of the stellar mass of the second most massive progenitor to the dominant progenitor should be less than 0.2.

We quantify the probability that a second most massive progenitor can be accreted by M31 analogues in the last 5 Gyr (Fig. S5). The probability of accreting a second most massive accreted satellite is about 40% (20%) for satellites with stellar masses greater than log (M_*) > 9.5 for Illustris (C13). This decreases to 10% (7%) for satellites with stellar masses greater than log (M_*) > 10. The difference in the two models can be attributed to the steeper slope of the stellar mass function around MW galaxies in the Illustris simulations compared to the Munich model.

6. Properties of the dominant progenitor

In the Illustris simulations, the majority of the dominant progenitors are gas-rich, star-forming galaxies with pronounced metallicity gradients. Nearly half of the galaxies contain at least a gas-to-stellar mass ratio of 0.8 in the inner parts of the galaxy (Fig S6). These accreted satellite galaxies are predominantly star-forming, having experienced a peak of star formation at z=1 (Fig S7). The star formation shuts down gradually from the outskirts to the inner parts of the galaxy (for an example, see Fig. 3 of the main paper) around 4 to 6 Gyr ago as they are being accreted by the galaxy. The center of the galaxy tends to be younger (and consequently more metal-rich). The centrally-concentrated star formation in these accreted satellites leads to differences in their stellar populations and strong metallicity gradients (See Fig S8).

7. Radial profiles of the debris field

The accreted stellar material contributed by the dominant progenitor determines the bulk properties of the accreted stellar component. In Fig. S9, we examine the major/minor axis profiles of the accreted stellar component for M31 analogues, as well as the accreted stellar profile contributed by the most massive accreted satellite. The median major axis profile of the accreted stellar component and the dominant progenitor can be well fit by an exponential profile beyond 20 kpc. On the other hand, the median minor axis profile of the accreted stellar profile as well as the dominant progenitor can be well approximated by a $R^{1/4}$ profile. We find that the median major/minor axis profiles of the accreted stellar component and the debris of the dominant accreted satellite are similar, but differ increasingly in the outer parts. The largest accreted satellite contributes more than 50% of the stellar material to the accreted stellar profile up to 45 kpc along the minor axis and up to 70 kpc along the major axis**.**

There is good agreement between the median minor axis profile of the accreted stellar component of M31 analogues and the observed minor axis surface brightness profile[24,25] of M31's stellar halo (inset of Fig 3). This comparison suggests that the minor axis profile beyond a projected distance of 10 kpc (fainter than μ_i ~ 25 mag/arcsec^2) appears to be predominantly accreted stellar material. At projected distances less than 10 kpc the surface brightness profiles are dominated by in-situ stellar material.

8. Tidal features

Tidal streams are a ubiquitous feature of a recent large merger. In Illustris, tidal features are found to survive 3-4 Gyr after the accretion of the galaxy. They extend out to a projected distance of ~100 kpc (see Fig. S10). They are predominately found in the plane of the disk.

Furthermore, the present day tidal features do not coincide with orbit of the incoming progenitor[38].

9. Dynamics of the debris field

The velocity dispersion of the accreted stellar component is driven by the dispersion of the debris field of the main accreted progenitor. Moreover, the projected velocity dispersion of the accreted stellar component of M31 analogues is similar to the observational constraints[39,40,41] of the velocity dispersion of the stellar halo from 15 to 65 kpc (Fig. S11).

In a significant fraction of our M31 analogues, the accreted stellar component is found to have a bulk rotation (Fig S12). A small fraction (< 10%) of these galaxies are found to possess no significant rotation, while a few galaxies exhibit counter-rotating disks. The peak of rotation (>150 km/s) is found at a distance of ~60 kpc along the major axis.

The significant rotation in the accreted stellar component is caused by the dominant progenitor. It is important to note that while the dominant progenitor may itself be rotating, the rotation in debris field is caused predominantly by its orbital motion as it is being accreted.

The velocity of the outer disk/inner stellar halo of M31 has been well studied[12]. Although a direct comparison of the predicted rotation and the observations is far from trivial, rotation velocities between 150-200 km/s were observed at galactocentric distances of 40-70 kpc along the major axis of M31[12]. This observed rotation is very similar to the predicted rotation velocities of the accreted stellar component of M31 analogues at similar distances.

10. Stellar populations of the debris field

Strong stellar population gradients are found in the accreted stellar component of M31 analogues. The main driver of these gradients are the stellar population gradients found in the dominant progenitor. The 2D median metallicity maps of the debris field (top panel of Fig S13) of only the dominant progenitor show significant differences of nearly 0.5 dex in [M/H] from place to place. The tidal features found in the outer parts contain preferentially the outer low-metallicity stars of the dominant progenitor. Moreover, most of tidal features contain a central metal-rich component with a larger metal-poor envelope.

Furthermore, the gradual shutdown of star formation in the dominant progenitor as it is being accreted by the main galaxy leads to variations in the stellar populations across the debris field. In general, accreted stars found at large galactocentric distances are older (>8 Gyr) than stars found at closer radii (< 5 Gyr) (see bottom panels of Fig. S13). The inner parts of the debris field of the accreted stellar component are significantly younger.

M31 has a significant fraction of younger stellar populations at a projected radius of 11 kpc, and that this fraction was larger at 11 kpc than at larger distances (21 and 35 kpc)[10,42], similar to the accreted debris of our M31 analogues. Given than the tidal features of the dominant progenitor have significantly lower metallicity than its central core, the metallicity of the visible part of the GSS should be lower than the central debris from its progenitor. Furthermore, the shutdown of

the bulk of star formation in the Giant Stellar Stream (GSS) at around 5 Gyr can be naturally explained as the cessation of star formation in the outer parts of the dominant progenitor.

11. M32p analogues

Galaxies like M32p are not uncommon in the local universe. We illustrate a few M32p analogues from the S4G survey[44,45] such that the stellar mass is between $10.2 < \log M^* < 10.6$, and that their central surface brightness is comparable to M32 within the inner 100 pc. For this, we first use the I-band central surface brightness profile of M32[15]. We ensure that the surface brightness of the S4G in the inner 100 pc is greater than 16 mag/arcsec^2 in [3.6] band. We found 8 galaxies (Fig. S14). Two of these galaxies (M82 and NGC 5195) are presently interacting with other galaxies.

12. Dynamical models of the Giant Stellar Stream

The Fardal framework models the dynamic interaction of the GSS with M31, predicting the mass of the progenitor ($\log M^* \sim 9.5 \pm 0.1$) at its last pericentric passage ($t_{acc} \sim 760 \pm 50$ Myrs ago; apocentre 55.5+/-4.5 kpc; pericentre 2.86+/-0.81 kpc) and the position of the remnant of the progenitor of the GSS (somewhere in the north-eastern shelf)[4].

While the model has successively predicted a number of qualitative features of the stream, the relaxation of the some of the model's assumptions will affect its quantitative predictions. First, the model assumes a shape of the potential parametrized by a simple parameter. In the outer parts of the halo, where the bulk of the GSS resides, there is a substantial uncertainty in the potential of M31 (including asphericity). This affects primarily the shape of the orbit (especially in the outer part) as well as the time of the last pericentric passage. Second, the models do not include the effects of dynamical friction, which leads to a loss of momentum and orbital energy of the progenitor, and an increase in the velocity dispersion of its debris. The amount of dynamical friction directly depends on the mass of the progenitor. The stellar mass of the progenitor predicted at the last pericentric passage according to the Fardal model is as large as the LMC. In contrast, dynamical friction is a vital ingredient in modeling the interaction of the LMC and the MW[46,47]. Even if the progenitor is tidally stripped of its DM, the ratio of its possible mass to the mass of M31 is sufficiently high enough ($>\sim 0.03$) for the effects of dynamical friction to become relevant. Third, the model further assumes that the progenitor was totally disrupted at its last pericentric passage. If part of the progenitor (e.g. the dense bulge) survived as a remnant, dynamical friction will differentially affect the core in contrast to the rest of the progenitor. This could imply that the remnant does not coincide with peak of the surface mass density of the rest of the disrupted progenitor. Fourth, for a such a large progenitor, holding the position of the M31 fixed can introduce a further bias in the phase-space orbit of the GSS. A dramatic effect was found in similar simulations between the LMC and the MW[48]. Fifth, systematic uncertainties in the distance estimates of the GSS as well as the uncertainty in the distance of the North eastern and Western shelves do not allow an accurate constraint on the orbit. Sixth, since the phase determination is sensitive to the inferred density of stars in the Western shelf and the GSS, systematic uncertainties in stellar density owing to unrelated M31 halo stars and MW foreground stars add further uncertainty to the phase estimate. Finally, the

proper motion of the stream is assumed to be minimal. This could possibly affect the outer path of the stream and the time of its last pericentric passage.

Given these model uncertainties, we believe that there are considerable uncertainties in the quantitative predictions of the model, which we expect could be off by a factor of 2 or more. M32 is moving radially in the direction of M31; its velocity (and projected radius) is consistent with the predicted caustics of both the North eastern shelf and the Western shelf. Accordingly, M32's position and radial velocity is consistent with that of the giant stellar stream passing from the North-eastern shelf and moving in the direction of the Western shelf. This would imply that the phase of the progenitor is at ~2 (using the phase convention of Fardal model which estimated it to be ~1.2). An increase of phase of the progenitor by a factor of 2 can easily increase the time of the last pericentric passage by a factor of ~2 bringing it close to ~1.5-2 Gyr, as well as argue for higher masses of the progenitor at its last pericentre. Such a revision would make the dynamical constraints of the progenitor of the GSS (the time of pericentric passage) consistent with the independent constraint of the end of the small burst in star formation found in the stellar populations of the GSS[10]. Moreover, the maximum stellar mass of the progenitor is likely to be much higher than at its last pericentric passage. Given the constraints on the timescale of the interaction from the star formation burst in M32 (~2 Gyr), M32p must have lost a significant amount of its stellar mass. This easily reconciles the mass estimates of M32p with those estimated by the Fardal model.

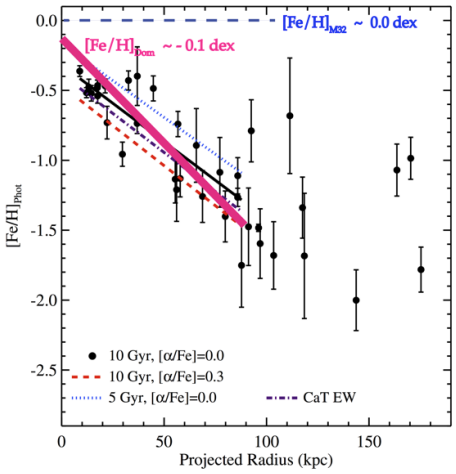

Fig. S1: Estimating the metallicity of the total accreted stellar component of M31 using the metallicity gradient of its stellar halo along the minor axis. The measurements of the stellar metallicity measurements along the minor axis are taken from the SPLASH survey. M32's metallicity is also indicated. The plot has been reproduced with permission from the authors[9].

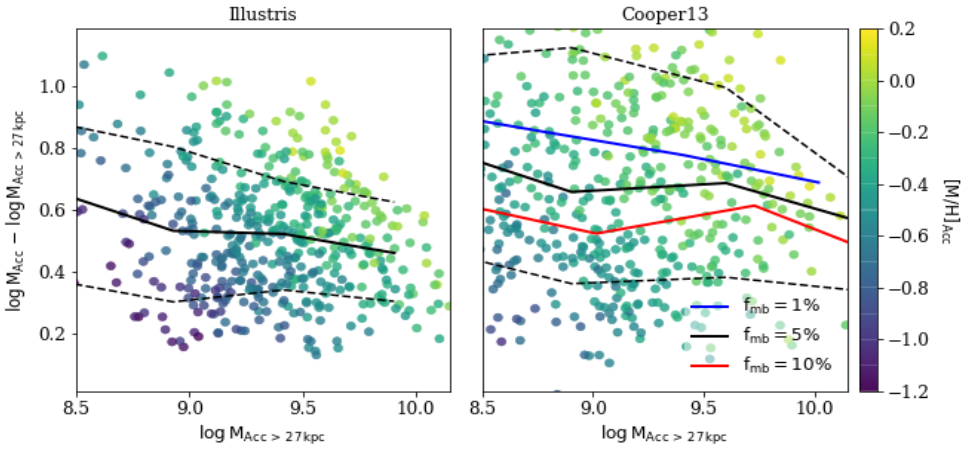

Fig. S2: The difference between the total accreted stellar and the accreted stellar mass measured beyond a projected radius of 27 kpc for M31-mass galaxies in both the Illustris (left) and the C13 simulations (right). In both panels, the solid line shows the median of the distribution while the dashed lines show the 16th and 86th percentile of the distribution. In the right panel, we show the median distribution for three levels of the tagging fraction of the most bound DM particles (1% 5% and 10% in blue, black and red respectively). On both panels, the points are colored by the metallicity of the accreted stellar component.

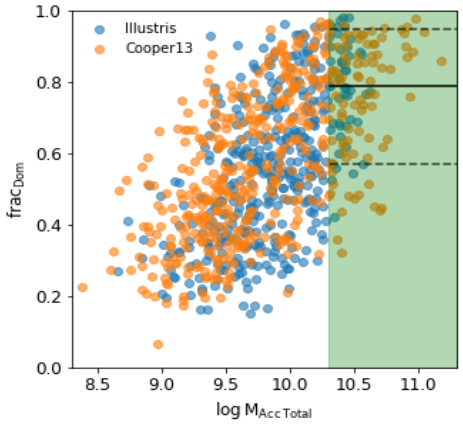

Fig. S3: The fraction of stellar mass contributed by the dominant progenitor to the accreted stellar component ($frac_{Dom}$) for M31-mass galaxies. M31 analogues are in the green shaded region. The black solid horizontal line is the median of $frac_{Dom}$ for Illustris M31 analogues. The dashed vertical lines show the 10 and 90 percentile of $frac_{Dom}$.

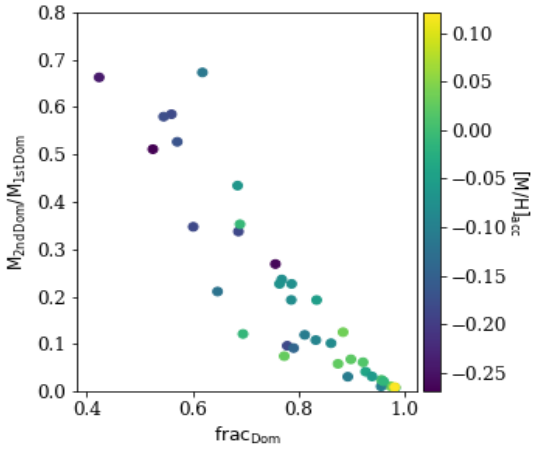

Fig. S4: The fraction of the second most massive accreted satellite to the most dominant accreted satellite as a function of $frac_{Dom}$ (the fraction of accreted stellar material contributed by the dominant progenitor) for M31 analogues from the Illustris simulations. The points are colored by the metallicity of the accreted stellar component (similar also to the metallicity of the most dominant accreted satellite).

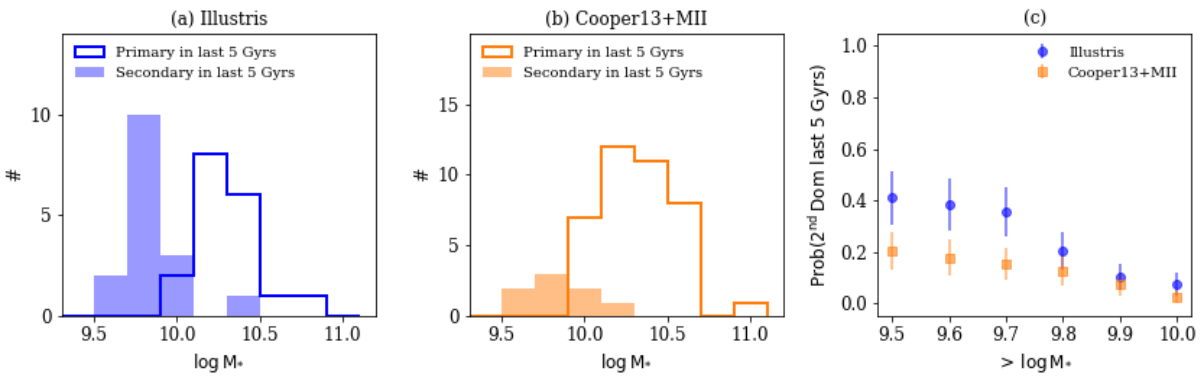

Fig. S5: Distribution of the properties of the second most massive recently-accreted satellite: A histogram of the most massive (primary) and the second most massive (secondary) satellites accreted by M31 analogues in the last 5 Gyr. Panel a represents the Illustris hydrodynamical simulation. Panel b represents the semi-analytic particle-tagging analysis of the Millennium II simulation. Panel c shows the probability that the second most massive progenitor could have contributed to the dominant features of the stellar halo of M31, assuming a given minimum threshold mass for the dominant progenitor (on the x axis).

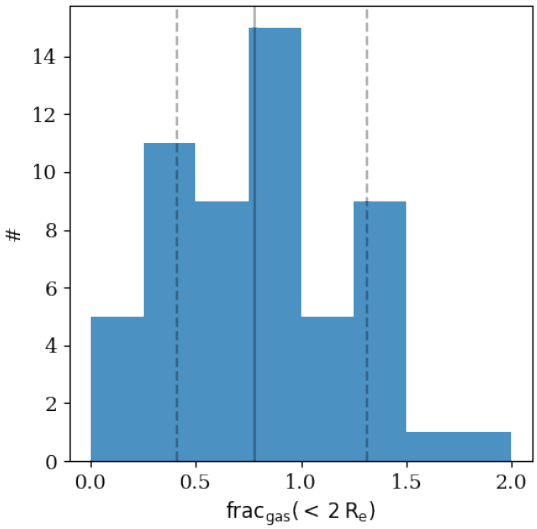

Fig. S6: Fraction of gas within 2 stellar mass radii of the dominant progenitor, when the galaxy had the maximum stellar mass (Illustris). The solid vertical line indicates median of the distribution, while the dashed vertical lines indicates 16 and 84 percentile of the distribution.

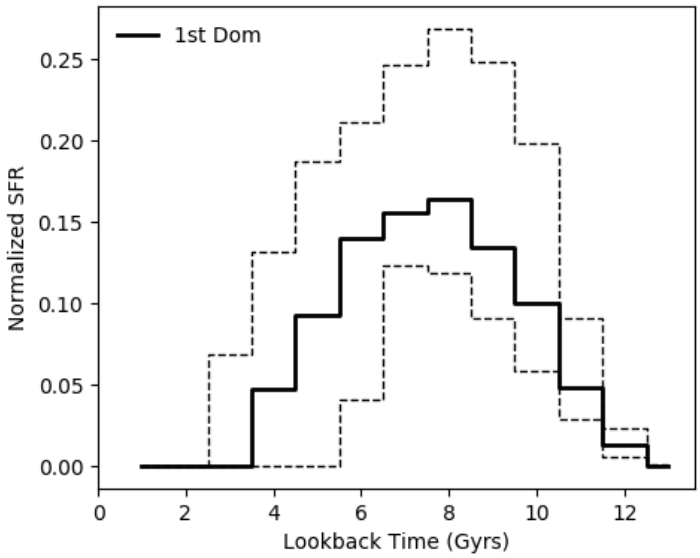

Fig. S7: Star-formation rate of the dominant progenitors of M31 analogues (Illustris) as a function of lookback time. The solid black line shows the median, while the dashed lines show the 10 and the 90% percentile of the SFR of the most dominant progenitor.

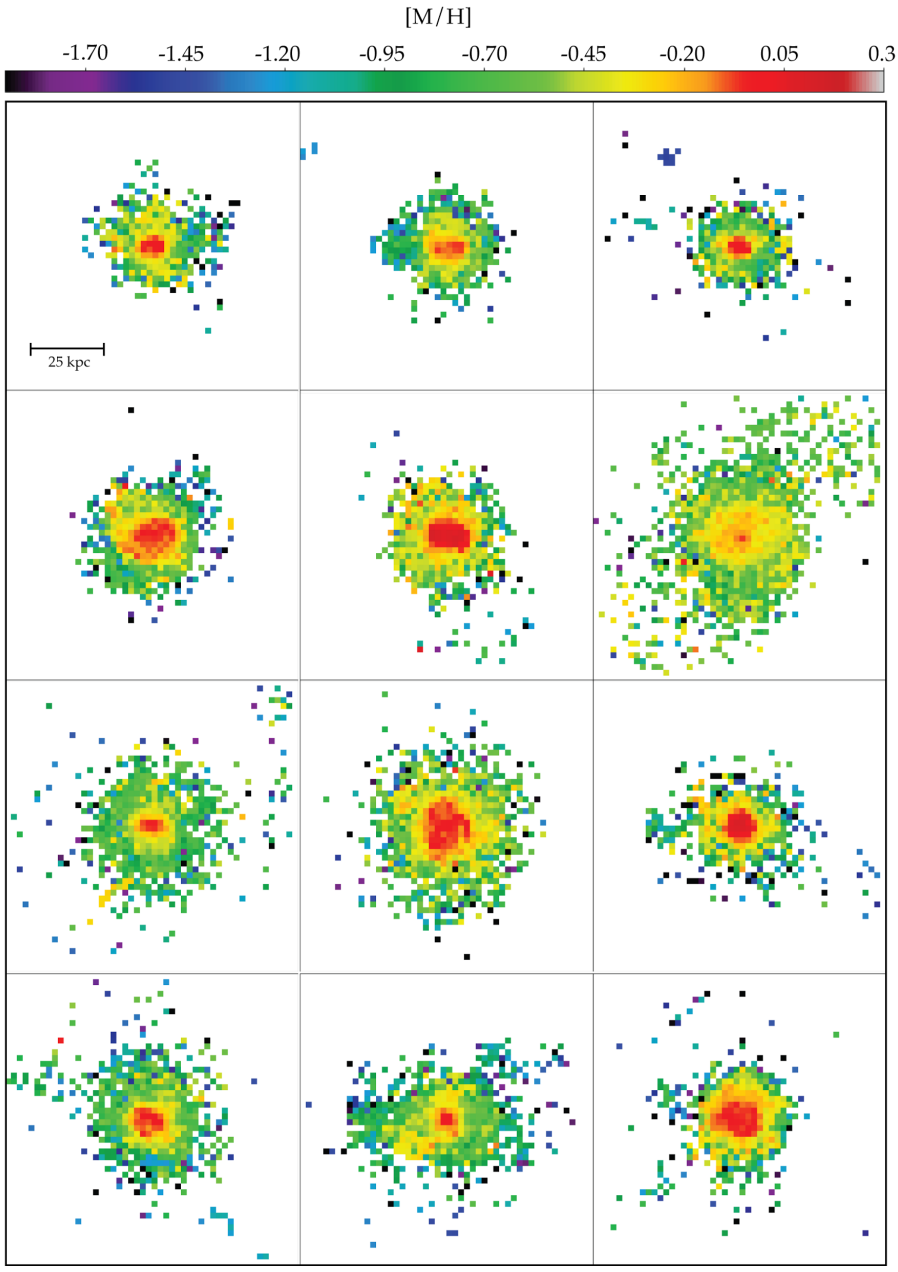

Fig. S8: Face-on metallicity maps of selected dominant satellites which are later accreted by the M31 analogues (Illustris). All of them have pronounced metallicity gradients.

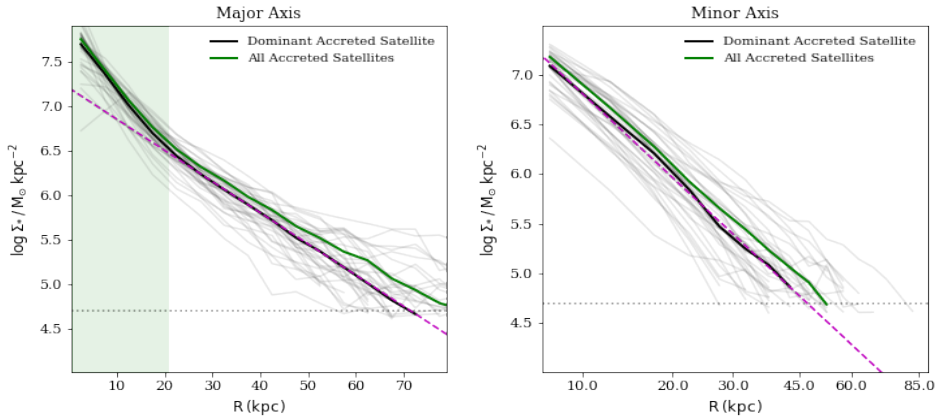

Fig. S9: The median radial profile of the stellar debris contributed by the most massive accreted satellite (solid black line) as well as contributed by all accreted satellites (solid green line) of M31 analogues from the Illustris simulations. The left panel shows the major axis while the right panel shows the minor axis. The light black lines show the individual radial profiles of the stellar debris of the most massive accreted satellites. In the left panel, the dashed magenta line is an exponential fit to the median radial profile of the most massive accreted satellite beyond 20 kpc. In the right panel, the dashed magenta line is a de Vaucouleurs fit to the median radial profile of the most massive accreted satellite. (The x-axis is linear in $R^{1/4}$). The horizontal dotted line is the mass resolution limit of the Illustris simulations.

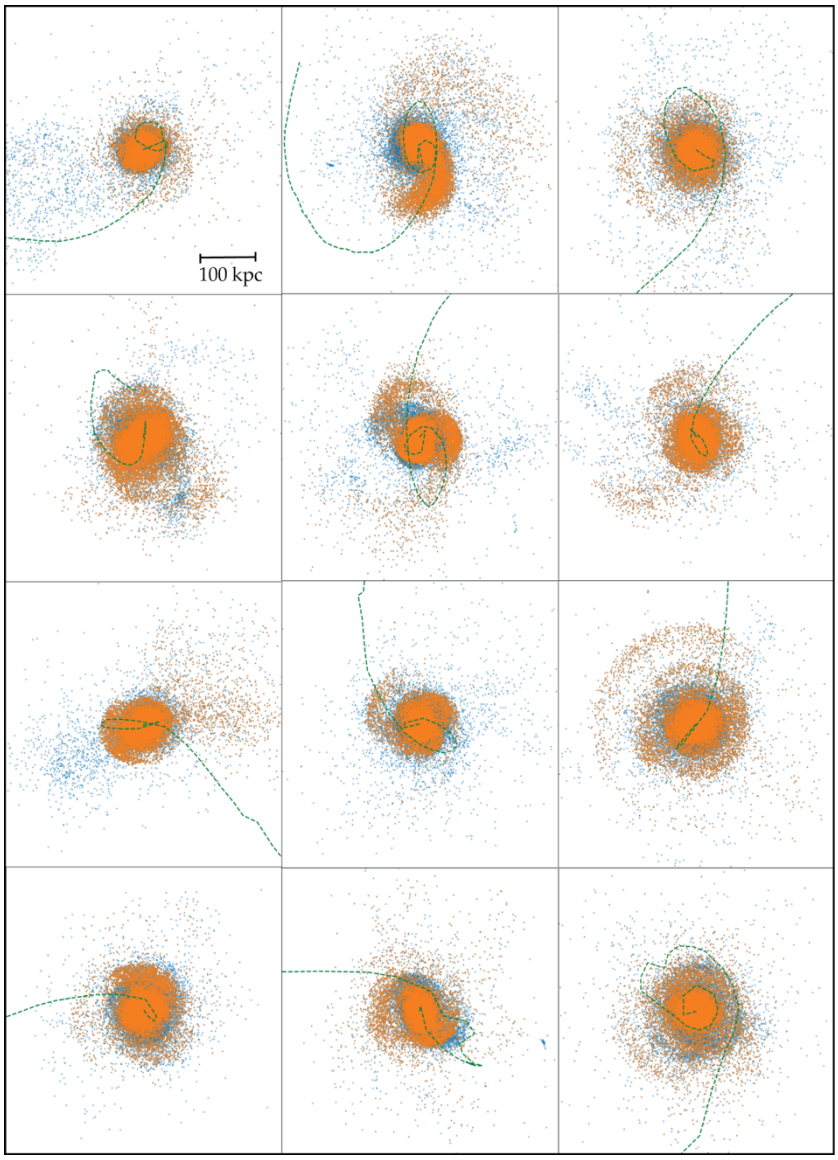

Fig. S10: Tidal features in M31 analogues (Illustris): A face-on view of the debris particles of the accreted stellar component. The blue dots represent all accreted stellar particles. The orange dots represent stellar particles which belong to the most dominant progenitor. The green line traces the projected path of the dominant progenitor as it is accreted by the galaxy.

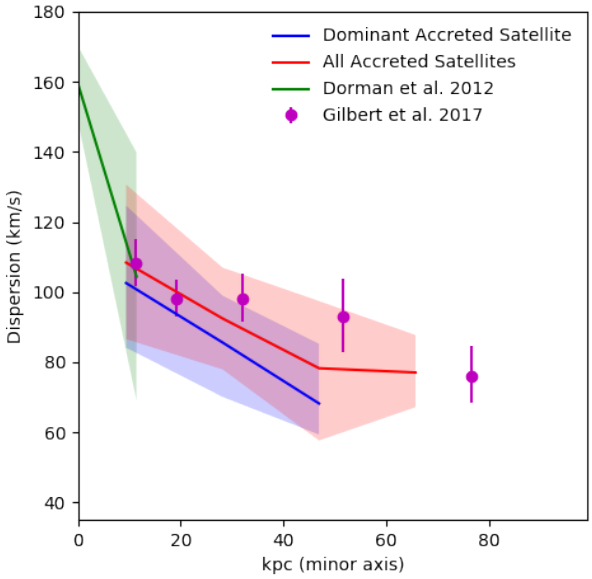

Fig. S11: Velocity dispersion profile along the projected minor axis for the dominant progenitor and the total accreted stellar component of M31 analogues from the Illustris simulations. The velocity dispersion decreases with radius. The shaded region shows the 10 and 90 percentile of the distributions. The velocity dispersion was calculated within a 10 x 10 kpc area.

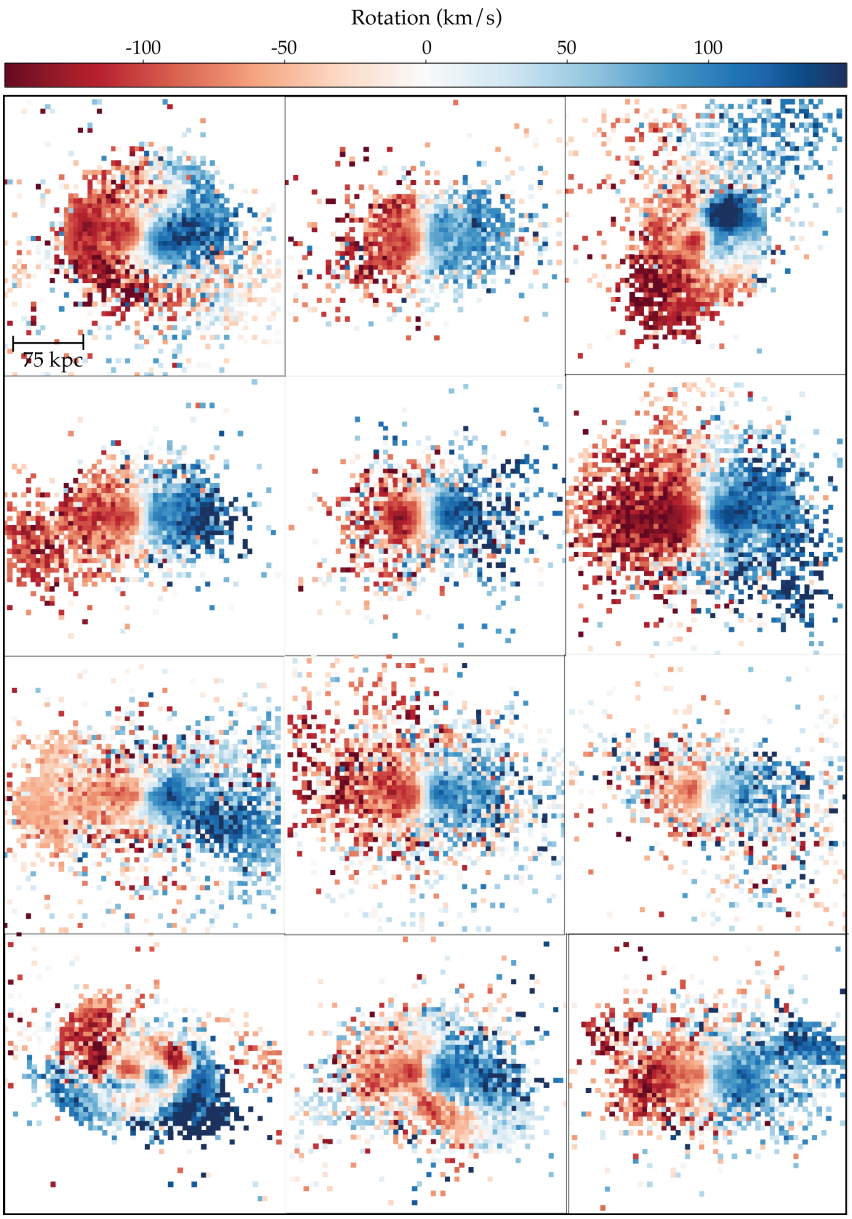

Fig. S12: 2D rotation maps of a nearly edge-on view of the accreted stellar component of selected M31 analogues (Illustris). The galaxies were tilted to an inclination angle of 78 degrees, in common with M31.

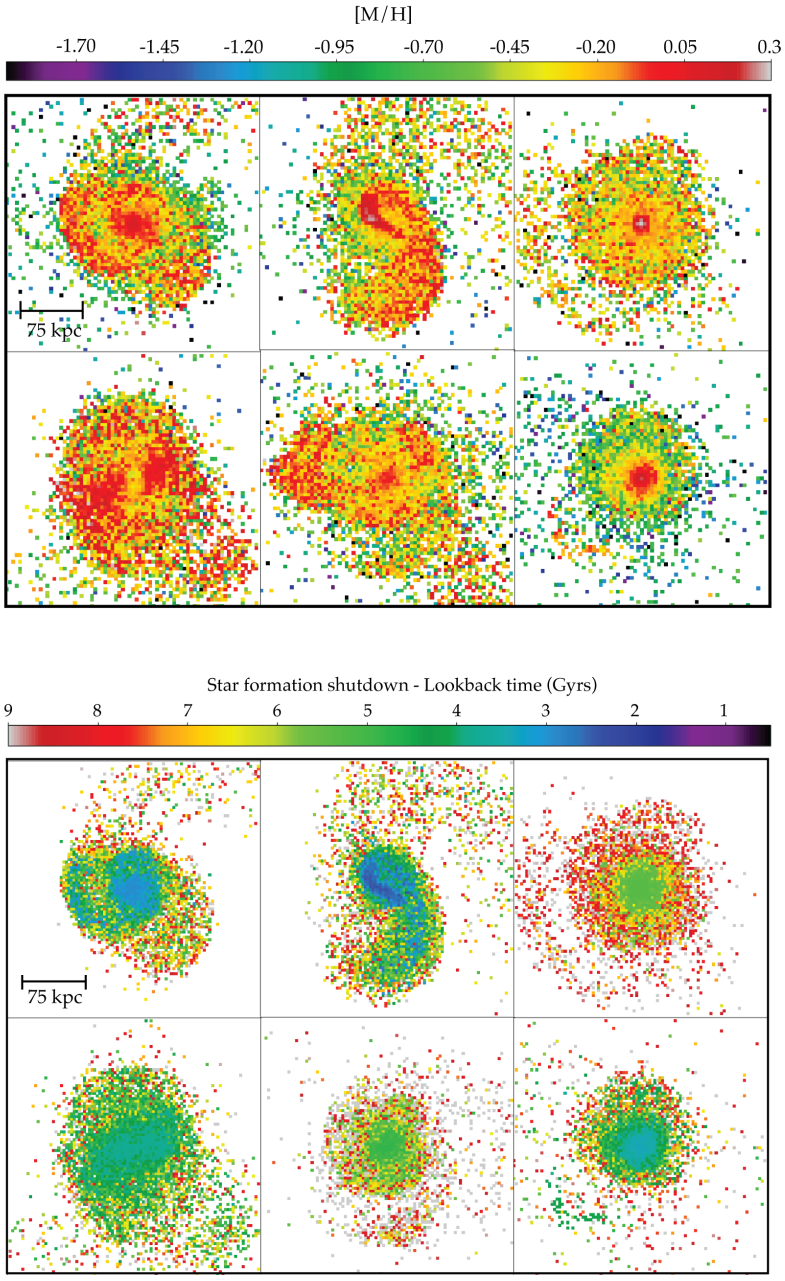

Fig. S13: Face on 2D maps of the median metallicity (top panel) and median lookback age for the shutdown of star formation (bottom panel) of the debris field of the dominant progenitor for a selection of M31 analogues (Illustris).

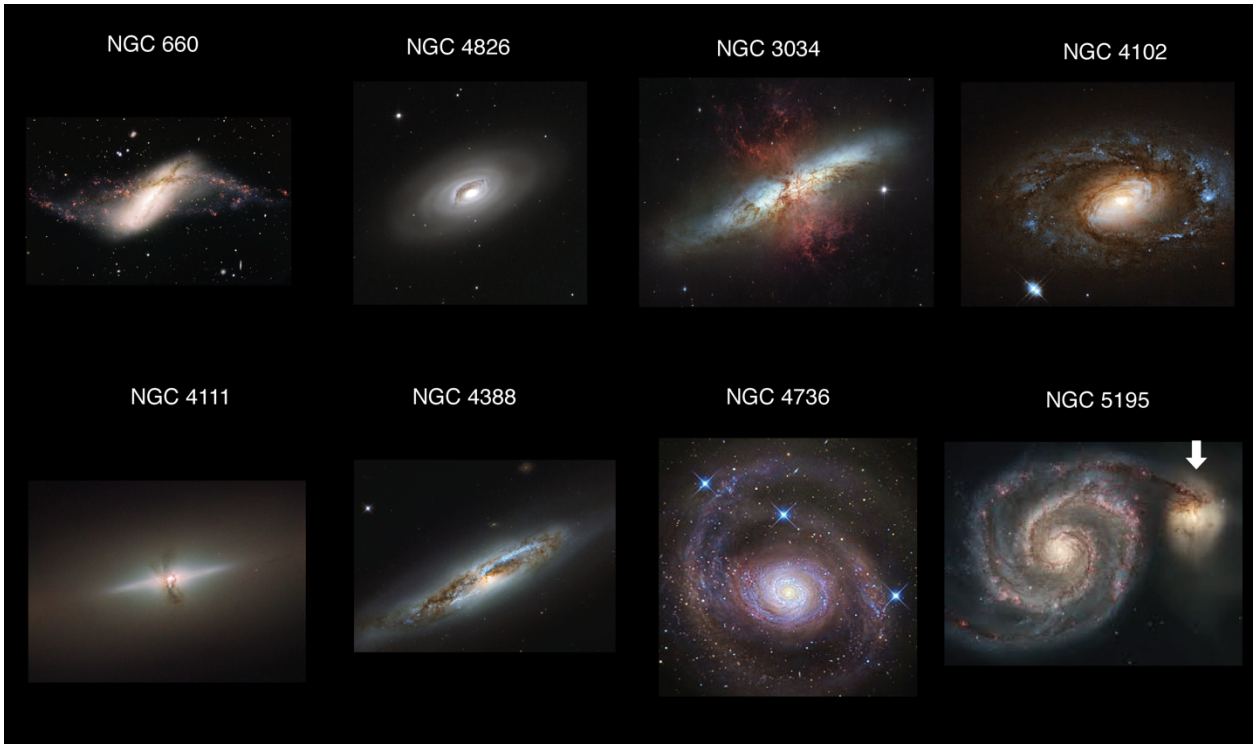

Fig. S14: M32p analogues chosen from the S4G survey. The images are taken from the public domain. Credits: NGC 660 (Gemini Observatory), NGC 4826 (NOAO/AURA/NSF), NGC 3034, NGC 4012, NGC 4111, NGC 4388 & NGC 5195 (ESA/Hubble & NASA), NGC 4736 (Jay Gabany).

References:

31. Penarrubia et al. A timing constraint on the (total) mass of the Large Magellanic Cloud, *Mon. Not. R. Astron. Soc.*, **456**, 54-58 (2016).
32. Tamm et al. Stellar mass map and dark matter distribution in M 31, *A&A*, **546**, 4-15 (2013).
33. Genel et al. Introducing the Illustris project: the evolution of galaxy populations across cosmic time, *Mon. Not. R. Astron. Soc*., **445**, 175-200 (2014).
34. Vogelsberger et al. Introducing the Illustris Project: simulating the coevolution of dark and visible matter in the Universe, *Mon. Not. R. Astron. Soc*., **444**,1518-1547 (2014).
35. Guo et al. From dwarf spheroidals to cD galaxies: simulating the galaxy population in a ΛCDM cosmology, *Mon. Not. R. Astron. Soc.*, **413**, 101-131 (2011).
36. Shen et al., The size distribution of galaxies in the Sloan Digital Sky Survey, *Mon. Not. R. Astron. Soc.*, **343**, 978-994 (2003).
37. Guo et al., Structural properties of central galaxies in groups and clusters, *Mon. Not. R. Astron. Soc.*, **398**, 1129-1149 (2009).
38. Fardal et al. Investigating the Andromeda stream - II. Orbital fits and properties of the progenitor, *Astrophys. J.*, **366**, 1012-1028 (2006).
39. Dorman et al., The SPLASH Survey: Kinematics of Andromeda's Inner Spheroid, *Astrophys. J*., **752**, 147-166 (2012).
40. Gilbert et al. Stellar Kinematics in the Complicated Inner Spheroid of M31: Discovery of Substructure along the Southeastern Minor Axis and Its Relationship to the Giant Southern Stream, *Astrophys. J*., **668**, 245-267 (2007).
41. Gilbert et al., Global Properties of M31's Stellar Halo from the SPLASH Survey III: Measuring the stellar velocity dispersion profile, arXiv:1711.02700v1 (2017).
42. Brown et al. The Extended Star Formation History of the Andromeda Spheroid at 21 kpc on the Minor Axis, *Astrophys. J*., 658, 95-98 (2007).
43. Brown et al. The Extended Star Formation History of the Andromeda Spheroid at 35 kpc on the Minor Axis, *Astrophys. J. L.*, **685**, 121 (2008).
44. Sheth et al. The Spitzer Survey of Stellar Structures in Galaxies, *PASP*, **122**, 1379-1414 (2010).
45. Muñoz-Mateos et al. The Spitzer Survey of Stellar Structure in Galaxies (S^4G): Stellar Masses, Sizes, and Radial Profiles for 2352 Nearby Galaxies, *Astrophys. J.S*, 219-231 (2015).
46. Mastropietro et al. The gravitational and hydrodynamical interaction between the Large Magellanic Cloud and the Galaxy, *Mon. Not. R. Astron. Soc*., **363**, 509-520 (2005).
47. Jethwa, Erkal & Belokurov, A Magellanic origin of the DES dwarfs, *Mon. Not. R. Astron. Soc.*, **461**, 2212-2233 (2016).
48. Gomez, F. et al., And Yet It Moves: The Dangers Of Artificially Fixing The Milky Way Center Of Mass In The Presence Of A Massive Large Magellanic Cloud., *Astrophys. J*., **802**, 128-144, (2015).